Rheologic constraints on the upper mantle from five years of postseismic deformation following the El Mayor-Cucapah earthquake

[fn]Department of Earth and Environmental

Abstract

Five years of post-seismic deformation following the Mw7.2 El Mayor-Cucapah earthquake reveals transient deformation that decays back

to its pre-earthquake trend after about 3 years at epicentral distances greater than $\sim$ 200 km. In the near-field, we observe rapid transience that decays to a sustained rate which exceeds its pre-earthquake trend. We attempt to determine the mechanisms driving this observed deformation, where we consider afterslip at seismogenic depths and viscoelastic relaxation in the lower crust and upper mantle as candidate mechanisms. We find that early, rapid, near-field deformation can be explained with afterslip on the portion of the fault that ruptured coseismically, while the later, sustained, near-field deformation can be explained with either continued afterslip in an effectively elastic lower crust, or lower crustal viscoelastic relaxation with a steady-state viscosity of $\sim 10^{19}$ Pa s. The trend in far-field deformation is best explained with a transient viscosity of $\sim 10^{18}$ Pa s in the upper mantle. We argue that a transient rheology in the mantle is preferable over a Maxwell rheology because it better predicts the decay of the postseismic deformation, and also because it does not conflict with the generally higher, steady-state viscosities inferred from studies of geophysical processes occurring over longer time-scales.

1 Introduction

Ground deformation in the years following a large ($\gtrsim$Mw7) earthquake provides insight into the mechanical behaviour of the crust and upper mantle. It has long been recognized that interpretations of post-seismic deformation can be ambiguous because multiple postseismic deformation mechanisms can have qualitatively similar surface expressions **?**, e.g.]Savage1990. Thanks to the dense geodetic network deployed throughout the 2000s as part of the Plate Boundary Observatory, the April 4, 2010, Mw7.2 El Mayor-

Cucapah earthquake in Baja California produced observable postseismic deformation at more GPS stations than any other earthquake in California to date. With such a large collection of data, we attempt to discern the mechanisms driving postseismic deformation fol- low- ing the El Mayor- Cucapah earth- quake, where we con- sider both af- ter- slip and vis- coelas- tic re- lax- ation in the lower crust and up- per man- tle as candidate mechanisms.

Previous studies which have modelled postseismic deformation following the El Mayor-Cucapah earthquake include **?**,

]Pol- litz2012, **?**,]Gonzalez- ortega2014, **?**,]Spin- ler2015, and **?**,]Rollins2015. Of these stud- ies, **?**,]Gonzalez- ortega2014 and **?**,]Rollins2015 have at- tempted to de- scribe the post- seis- mic de- formation with afterslip in an elastic half-space. **?**,]Gonzalez-ortega2014 described five months of post-seismic deformation, observed by near-field ($\lesssim$

50 km from the rupture) campaign GPS and InSAR, with afterslip and contraction on the coseismically ruptured fault. **?**,]Gonzalez-ortega2014 noted

that their preferred model underestimated the GPS displacements for stations $\gtrsim$ 25 km from the rupture and suggested that it could be the re-sult of un-mod-elled vis-coelas-tic re-lax-ation. Us-ing con-tin-u-ous GPS sta-tions, which are mostly north of rup-ture zone, **?**,]Rollins2015 found that three years of post-seismic deformation can be adequately explained by afterslip, albeit with an implausibly large amount of slip inferred on the least constrained, southernmost fault segment. Here, we suggest the afterslip inferred by **?**,]Rollins2015 may have been acting as a proxy for distributed relaxation in the upper mantle.

?,]Pollitz2012, **?**,]Rollins2015 and **?**,]Spinler2015 have explored viscoelastic relaxation in the lower crust and upper mantle as a potential postseismic deformation mechanism. The rheology of the crust and mantle is largely unknown and so modelling post-seismic deformation with viscoelastic relaxation requires one to assume a rheologic model and then find the best fitting rheologic parameters. The inference of these rheologic parameters is a computationally expensive nonlinear inverse problem which is typically approached with a forward modelling grid search method. Consequently, a simplified structure for the lithosphere must be made to minimize the number of rheologic parameters that need to be estimated. For example, it is commonly assumed that the lithosphere consists of only three homogeneous, Maxwell viscoelastic layers, which may be an inadequate representation of the lithosphere **?**,]Riva2009,Hines2013. To further reduce the model space dimensions being search, it is also necessary to make simplifying assumptions about the nature of afterslip. For example, one can assume a frictional model for afterslip and parametrize afterslip in terms of the unknown rheologic properties of the fault **?**, e.g.]Johnson2009,Johnson2004. One can also assume that afterslip does not persist for more than a few months and then model the later post-seismic deformation assuming it to be the result of only viscoelastic relaxation **?**, e.g.]Pollitz2012,Spinler2015. However, postseismic afterslip in similar tectonic settings has been observed to persist for decades following earthquakes **?**,]Cakir2012,Cetin2014. Neglecting to allow for sustained afterslip as a postseismic mechanism could then lead to a biased inference of lithospheric viscosity. Indeed, the preferred viscoelastic model from **?**,]Pollitz2012 significantly underestimates near-field deformation, which could be indicative of unmodelled continued afterslip.

In this study, we assume that both afterslip and viscoelastic relaxation can contribute to postseismic deformation. Modelling both of these mechanisms creates a high dimensional model space that must be searched with non-linear op-ti-miza-tion meth-ods. We first de-velop an ini-tial post-seis-mic model us-ing the method de-scribed in **?**,]Hines2016. This method simultaneously estimate the afterslip and effective lithospheric viscosity structure necessary to describe the first 0.8 years of postseismic deformation following the El Mayor-Cucapah earthquake. We then use the inferred effective viscosity structure to create a suite of post-seismic models which are tested against the available 5 years of post-seismic data. Of the suite of models tested, we find that postseismic deformation following the El Mayor-Cucapah earthquake can be explained with afterslip beneath the Sierra Cucapah, a Zener rheology upper mantle with a transient viscosity that decays from 5×10^{18} Pa s to 1×10^{18} Pa s at 120 km depth, and a rela-tively stronger lower crust.

2 Data Processing

We use continuous GPS position time series provided by University Navstar Consor-

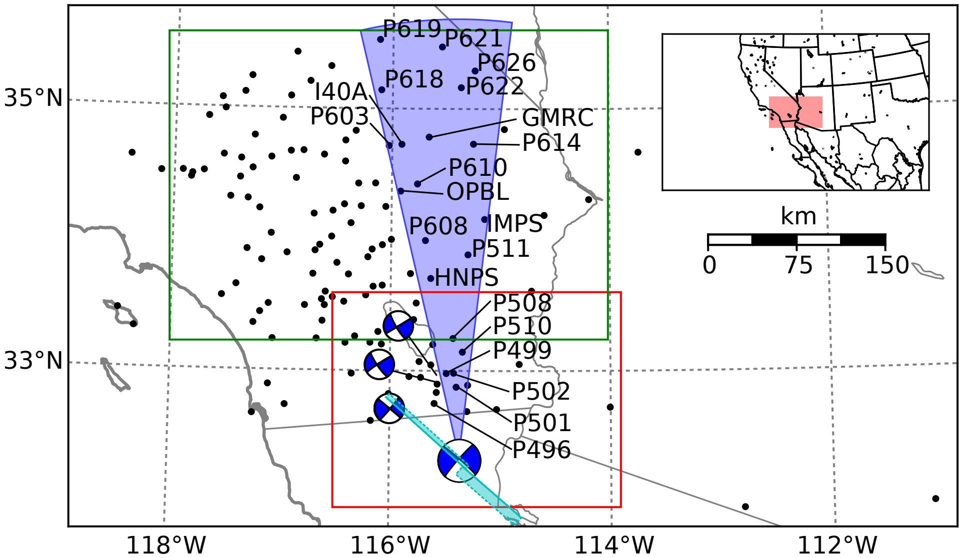

Figure 1. Map of the region considered in this study. The large focal mechanism is for the El Mayor-Cucapah earthquake and the three small focal mechanisms

tium (UN- AVCO) for sta- tions within a 400 km ra- dius about the El Mayor- Cucapah epi- cen- tre. We col- lec- tively de- scribe the co- seis- mic and post- seismic dis- place- ments re- sult- ing from the El Mayor- Cucapah earth- quake as $u_{\mathrm{post}}(t)$. We con- sider the GPS po- si- tion time se- ries, $u_{\mathrm{obs}}(t)$, to be the su- per-

po-
si-
tion
of
$u_{\mathrm{post}}(t)$,
sec-
u-
lar
tec-
tonic
de-
for-
ma-
tion,
an-
nual
and
semi-
annual
os-
cil-
la-
tions,
and
co-
seis-
mic
off-
sets
from
sig-
nif-
i-

cant earthquakes over the time span of this study. The June 14, 2010, Mw5.8 Ocotillo earthquake and the Brawley swarm, which included an Mw5.5 and an Mw5.3 event on

August 26, 2012, (Figure **??**) are the only earthquakes that produced noticeable displacements in any of the time series. We treat the displacements re- sult- ing from the Braw- ley swarm as a sin- gle event be- cause the time se- ries are pro- vided by UN- AVCO as daily so- lu- tions. Al- though the Ocotillo earth- quake had its own se- ries of af- ter- shocks **?**,]Hauks- son2011, nei- ther the Ocotillo earth- quake nor the Braw- ley swarm pro- duced de- tectable post- seismic deformation and we model displacements resulting from these events with a Heaviside function, $H(t)$. We then model $u_{\text{obs}}(t)$ as

$$u_{\text{obs}}(t) = u_{\text{pred}}(t) + \epsilon \quad (1)$$

where

$$
\begin{aligned}
u_{\mathrm{pred}}(t) = & u_{\mathrm{post}}(t) H(t - t_{\mathrm{emc}}) + c_0 + c_1 t + \\
& c_2 \sin(2\pi t) + c_3 \cos(2\pi t) + c_4 \sin(4\pi t) + c_5 \cos(4\pi t) + \\
& c_6 H(t - t_{\mathrm{oc}}) + c_7 H(t - t_{\mathrm{bs}}).
\end{aligned}
\tag{2}
$$

In the above equations, t_{emc}, t_{oc} and t_{bs} are the times of the El Mayor-Cucapah earthquake, Ocotillo earthquake, and the Brawley swarm, respectively, c_0 through c_7 are unknown coefficients, and ϵ is the observation noise. We only estimate jumps associated with the

Ocotillo earthquake and Brawley swarm for stations within 40 km of their epicentres.

Stations which recorded displacements that clearly cannot be described by the aforementioned processes are not included in our analysis. This includes stations in the Los Angeles basin, where anthropogenic formation can be larger than the post-seismic signal that we are trying to estimate **?**,]Bawden2001,Argus2005 . In order to ensure an accurate estimation of the secular deformation, we only use stations that were installed at least six months prior to El Mayor-Cucapah earthquake. Several GPS stations were installed after the El Mayor-Cucapah earthquake to improve the spatial resolution of postseismic deformation **?**,]Spinler2015 and it is possible to subtract secular velocities derived from elastic block models **?**, e.g.]Meade2005 from veloc- i- ties recorded at the newly in- stalled sta- tions to get an es- ti- mate of post- seis- mic ve- loc- i- ties. How- ever, we use co- seis- mic and post-seismic displacements, rather than velocities, in our inverse method described in Section **??**. We use displacements because estimating velocities from an already noisy displacement time series can introduce significant aleatoric and epistemic uncertainties depending on exactly how the estimation is done. This modelling choice prevents us from using the newly installed stations in Baja California for our analysis.

The October 16, 1999, Mw7.1 Hector Mine earthquake, which occurred about 270 km north of the El Mayor-Cucapah epicentre, produced transient postseismic deformation which we do not wish to model, either mechanically or through empirical line fitting. We thus restrict our analysis to deformation observed six years after the Hector Mine earthquake, which is when postseismic velocalities at sites proximal to the Hector Mine epicentre are approximately constant **?**,]Savage2009. When appraising our model fit in Section **??**, we see some systematic residuals in the vicinity of the Hector Mine epicentre, which may be the result of errors in the assumption that the trend in Hector Mine postseismic deformation is linear after six years.

Studies of postseismic defor- ma- tion typ- i- cally as- sume a para- met- ric form for $u_{\mathrm{post}}(t)$, such as one with a log- a- rith- mic or ex- po- nen- tial time de- pen- dence

?, e.g.]Savage2005a. However, by assuming a logarithmic or exponential form of $u_{\mathrm{post}}(t)$ we run the risk of over fitting the GPS time series and in- fer- ring a non- existent post- seis- mic sig- nal. We there- fore do not as- sume any para- met- ric form for $u_{\mathrm{post}}(t)$ and rather treat it as integrated Brownian motion, so that

$$\dot{u}_{\text{post}}(t) = \sigma^2 \int_0^t w(s)ds, \quad (3)$$

where $w(t)$ is white noise and the variance of $\dot{u}_{\text{post}}(t)$ increases linearly with time by a factor of

σ^2. We use a Kalman fil- ter- ing ap- proach to es- ti- mate $u_{\text{post}}(t)$ and the un- known pa- ram- e- ters in eq. (**??**). In the con- text of Kalman filtering, our time varying state vector is

$$\mathbf{X}(t) = [u_{\mathrm{post}}(t), \dot{u}_{\mathrm{post}}(t), c_0, ..., c_7] \quad (4)$$

and eq. (**??**) is the observation function which maps the state vector to the GPS observations. We initiate the Kalman filter by assuming a prior estimate of $\mathbf{X}(t)$ at the first time epoch, denoted $\mathbf{X}_{1|0}$, which has a sufficiently large covariance, denoted $\boldsymbol{\Sigma}_{1|0}$, to effectively make our prior uninformed. For each time epoch, t_i, Bayesian linear regression is used to incorporate GPS derived estimates of displacement with our prior estimate of the state, $\mathbf{X}_{i|i-1}$, to form a posterior estimate of the state, $\mathbf{X}_{i|i}$, which has covariance $\boldsymbol{\Sigma}_{i|i}$.

We then use the posterior estimate of the state at time t_i to form a prior estimate of the state at time t_{i+1} through the transition function

$$\mathbf{X}_{i+1|i} = \mathbf{F}_{i+1}\mathbf{X}_{i|i} + \delta_{i+1} \tag{5}$$

where

$$\mathbf{F}_{i+1} = \begin{bmatrix} 1 & (t_{i+1} - t_i) & \mathbf{0} \\ 0 & 1 & \mathbf{0} \\ \mathbf{0} & \mathbf{0} & \mathbf{I} \end{bmatrix} \tag{6}$$

and δ_{i+1} is the process noise, which has zero mean and covariance described by

$$\mathbf{Q}_{i+1} = \sigma^2 \begin{bmatrix} \frac{(t_{i+1}-t_i)^3}{3} & \frac{(t_{i+1}-t_i)^2}{2} & \mathbf{0} \\ \frac{(t_{i+1}-t_i)^2}{2} & (t_{i+1}-t_i) & \mathbf{0} \\ \mathbf{0} & \mathbf{0} & \mathbf{0} \end{bmatrix}. \tag{7}$$

The covariance of the new prior state, $\mathbf{X}_{i+1|i}$, is then described by

$$\mathbf{\Sigma}_{i+1|i} = \mathbf{F}_{i+1}\mathbf{\Sigma}_{i|i}\mathbf{F}_{i+1}^T + \mathbf{Q}_{i+1}. \tag{8}$$

This process is repeated for

each of the N time epochs at which point we use Rauch-Tung-Striebel smoothing **?**,]Rauch1965 to find $\mathbf{X}_{i|N}$, which is an estimate of the state at time t_i

that incorporates GPS observation for all N time epochs. Our final estimates of $u_{\text{post}}(t)$ are used in subsequent analysis, while the remaining components of the state vector are considered nuisance parameters. In the interests of computational tractability, we down sample our smoothed time series from daily solutions down to weekly solutions.

The smoothness of $u_{\text{post}}(t)$ is controlled by the chosen value of σ^2, which describes how rapidly we expect postseismic displacements to vary over time. Setting σ^2 equal to zero will effectively result in modelling $u_{\mathrm{post}}(t)$ as a straight line which is insufficient to describe the expected transient behaviour in post-seismic deformation. The other end member, where σ^2 is infinitely large, will result in $u_{\mathrm{pred}}(t)$ over fitting the data. While one can use a maximum likelihood based approach for pick- ing σ^2 **?**, e.g.]Segall1997, we rather take a sub- jec- tive ap- proach and choose a value for σ^2 that is just large enough to faith- fully de- scribe the observed deformation at the most near-field station in our study, P496, which exhibits the most pronounced rapid changes in velocity. This ensures that σ^2 will be sufficiently large so that our estimate of $u_{\mathrm{post}}(t)$ does not smooth out potentially valuable postseismic signal at the remaining stations. We find that using $\sigma^2 = 0.05\mathrm{m}^2/\mathrm{yr}^3$ adequately describe all but the first week of postseismic deformation at station P496, which gets in- cor- po- rated into our es- ti- mate of co- seis- mic dis- place- ments (Fig- ure **??**). By down sam- pling, we im- plic- itly as- sume that the first week of deformation is overwhelmingly the result of afterslip and this afterslip is lumped into our estimates of coseismic slip. **?**,]Freed2007a noted that postseismic deformation can be observed at distances greater than 200 km from the Hector Mine earthquake and, after filtering the time series for stations up to 400 km from the El Mayor-Cucapah epicentre, we also clearly see far reaching post-seismic transient deformation (Figure **??**).

It is important to note that the shown uncertainties in $u_{\mathrm{post}}(t)$ do not account for the non-negligible

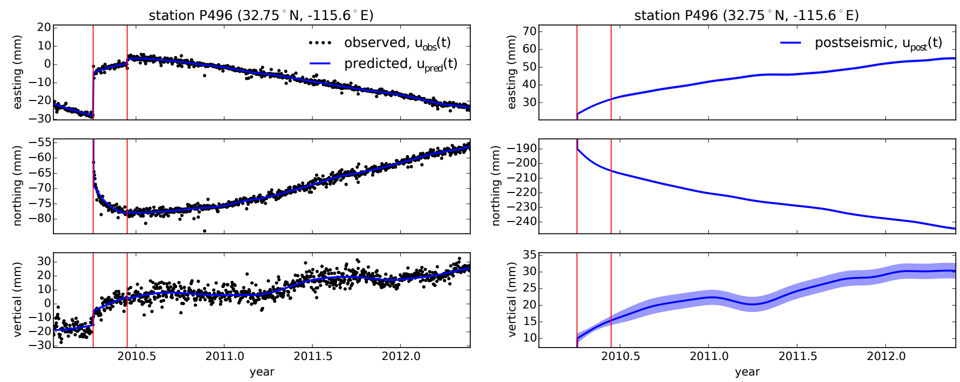

Figure 2. Left panels show GPS time series from UNAVCO (black) and the predicted displacement (blue) from eq. (**??**) for a near-field station. Red lines indicate the times of the El

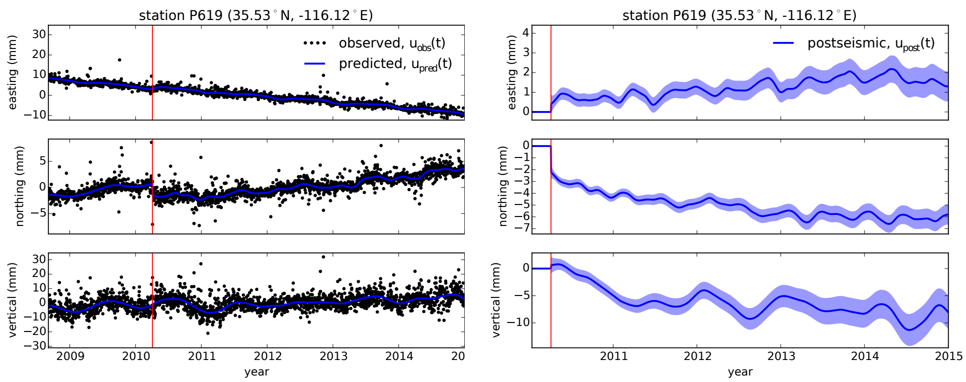

Figure 3. same as Figure **??** but for a far-field station.

epistemic uncertainty in eq. (**??**). For example, we assume a constant rate of secular deformation, which appears to be an ap- pro- pri- ate ap- prox- i- ma- tion for all but per- haps the sta- tions clos- est to the Hec- tor Mine epi- cen- tre, as noted above. Also, our model for seasonal deformation in eq. (**??**) assumes a constant amplitude over time, which means that any yearly variability in the climatic conditions could introduce systematic residuals **?**,]Davis2012. Indeed, it would be more appropriate to consider the seasonal amplitudes

c_2– c_5 in eq. (**??**) as stochastic variables **?**,]Murray2005. By using constant seasonal amplitudes our estimate of $u_{\text{post}}(t)$ seems to describe some of the unmodelled annual and semi-annual oscillations (e.g. Figure **??**).

We show in Figures **??** and **??** the near and far-field postseismic displacements accumulated over the intervals 0-0.8 years, 0.8-3.0 years, and 3.0-5.0 years, as well as the coseismic displacements. In the far-field to the north, we can see south trending displacements for the first 3 years following the earthquake at stations as far as ~400 km from of the El Mayor Cu- ca- pah epi- cen- tre. These dis- place- ments are most pro- nounced along the di- rec- tion of the El Mayor- Cucapah P axis. A similar eastward trend can be seen in the few far-field stations along the T axis in Arizona. After 3 years, the trend in far-field post-seismic deformation is barely perceptible. The vertical deformation in the far-field is difficult to attribute to post-seismic processes. Most far-field stations display an initial subsidence for the first year after the El Mayor-Cucapah earthquake followed by continued uplift. This trend in vertical deformation can be observed in all three of the quadrants where postseismic data is available, which means that the vertical deformation does not exhibit an anti-symmetric quadrant pattern, as would be expected for postseismic processes. Although we use vertical deformation in our analysis in Section **??**, we do not put an emphasis on trying to describe the vertical deformation as it likely does not have postseismic origins.

The near-field postseismic deformation is

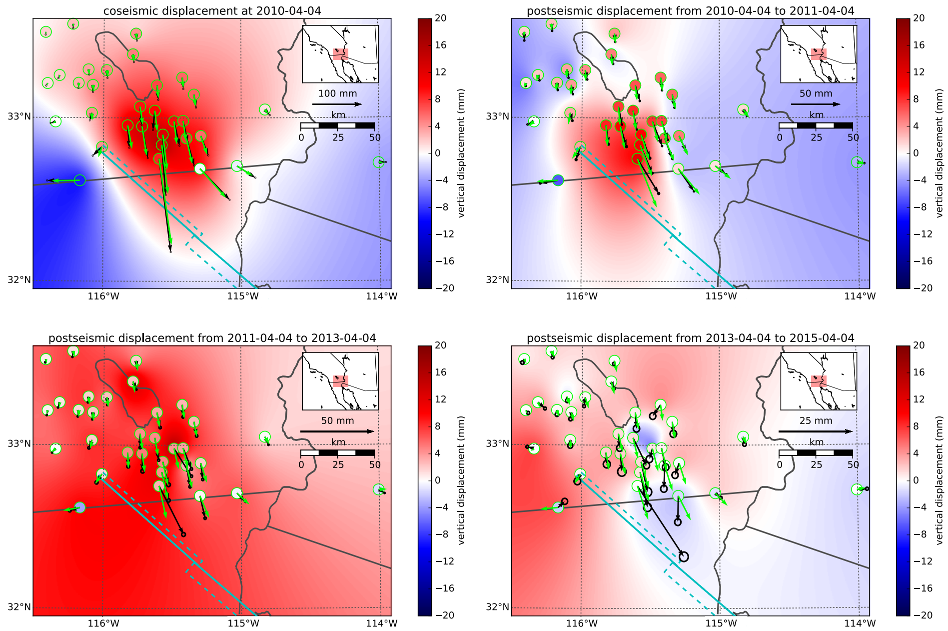

Figure 4. Near-field coseismic and postseismic displacements (black) as well as predicted displacements for our preferred model from Section **??** (green). Observed

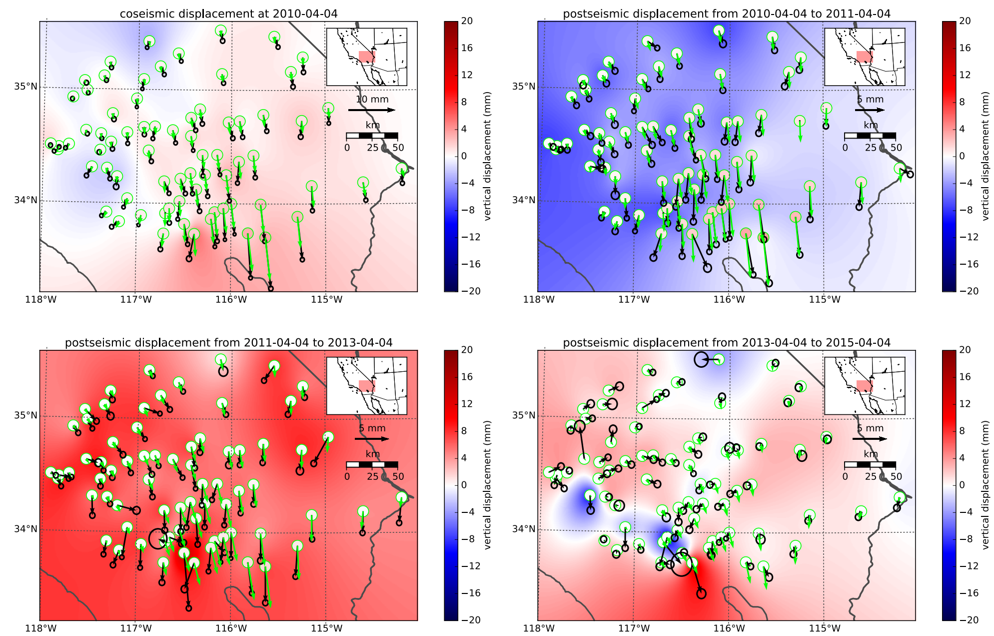

Figure 5. Same as Figure **??** but for far-field stations.

notably sustained when compared to the far-field deformation. Namely, the station in this study which is closest to the El Mayor-Cucapah epicentre, P496, has been moving at a steady rate of ∼ 1.5 cm/yr to the south since ∼ 1 year after the El Mayor-Cucapah earthquake. Vertical postseismic deformation in the near-field does display a quadrant pattern which is consistent with the coseismic vertical deformation, suggesting that it is resulting from tectonic processes. However, the vertical postseismic signal is only apparent for the first year after the earthquake (Figure **??**). As with the far-field deformation, there is a general trend of uplift in the near-field after ∼ 1 year, which we do not consider to be related to postseismic processes.

3 Postseismic Modeling

In this paper, we seek to

depth (km)	λ (GPa)	μ (GPa)	η_{eff} (10^{18} Pa s)	μ_{k}/μ
0-5	24.0	24.3	-	-
5-15	35.2	35.4	-	-
15-30	41.8	41.9	44.3	0.0
30-60	61.0	60.8	5.91	0.375
60-90	61.0	60.8	1.99	0.375
90-120	61.0	60.8	1.31	0.375
120-150	61.0	60.8	1.10	0.375
150-∞	61.0	60.8	1.07	0.375

Table 1. Assumed and estimated material properties. λ and μ are assumed known *a priori*, η_{eff} is estimated in Section **??** and $\frac{\mu_k}{\mu}$ are the optimal shear moduli ratios

find the mechanisms driving 5 years of postseismic deformation following the El Mayor-Cucapah earthquake. We consider afterslip and viscoelastic relaxation in the lithosphere and asthenosphere as candidate mechanisms. Poroelastic rebound has also been used to model post-seis- mic de- for- ma- tion **?**, e.g.]Jonsson2003; how- ever, **?**,]Gonzalez- ortega2014 sug- gest that any con- tri- bu- tion to post- seis- mic de- for- ma- tion from poroe- las- tic rebound would be negligible. Furthermore, we consider stations which are sufficiently far away from the main rupture that poroelastic rebound should be insignificant.

We estimate coseismic and time-dependent postseismic fault slip, both of which are assumed to occur on a fault geometry modified from **?**,]Wei2011. Field studies **?**,]Fletcher2014 and LIDAR observations **?**,]Oskin2012 have revealed a significantly more complicated fault geometry than what was inferred by **?**,]Wei2011, especially within the Sierra Cucapah. However, we find that a rel- a- tively sim- ple co- seis- mic fault ge- om- e- try based on **?**,]Wei2011 is ad- e- quate be- cause most of the sta- tions used in this study are sufficiently far from the El Mayor-Cucapah rupture zone that they are insensitive to the details in the fault geometry found by **?**,

]Fletcher2014 and **?**,]Oskin2012. The fault geometry used in this study (Figure **??**) consists of the two main fault segments inferred by **?**,]Wei2011, where the northern segment runs through the Sierra Cucapah up to the US-Mexico border and the southern segment is the Indiviso fault which extends down to the Gulf of California. Both segments extend from the surface to 15 km depth. We extend the northern segment by 40 km to the northwest, motivated by the clustering of aftershocks on the northern tip of the coseismic rupture zone **?**,]Hauksson2011,Kroll2013.

This extended fault segment was also found to be necessary by **?**,]Rollins2015 and **?**,]Pollitz2012 in order to describe the postseismic deformation.

3.1 elastic inversion

We consider a variety of rheologic models for the lower crust and upper mantle. The simplest

rhe-
o-
logic
model
is
to
con-
sider
them
to
be
ef-
fec-
tively
elas-
tic
and
isotropic.
In
such
case,
the
rhe-
o-
logic
pa-
ram-
e-
ters
con-
sist
of
the

Lamé parameters, λ and μ, which are reasonably well known and we use the values listed in Table **??** throughout this paper. The only

un-
known
is
the
dis-
tri-
bu-
tion
of
fault
slip,
which
can
be
eas-
ily
es-
ti-
mated
from
post-
seis-
mic
de-
for-
ma-
tion
through
lin-
ear
least
squares.
Us-

ing a sub-set of the GPS sta-tions con-sid-ered in this study, **?**,]Rollins2015 found that post-seis-mic de-for-ma-tion fol-low-ing the El Mayor-Cucapah

earth-
quake
can
be
ex-
plained
with
af-
ter-
slip
on
the
co-
seis-
mic
fault
plane
and
they
did
not
re-
quire
any
vis-
coelas-
tic
re-
lax-
ation
to
de-
scribe

the observations. We also perform an elastic slip inversion but we use GPS stations within a larger radius about the El Mayor-Cucapah epicentre (400 km instead of $\sim$200 km). Our forward problem describing predicted postseismic deformation, u_{pred}, in terms of time dependent fault slip, s, is

$$u_{\text{pred}}(x,t) = \int_F s(\xi,t)g(x,\xi)d\xi \quad (9)$$

where $g(x,\xi)$ is elastic Green's function describing displacement at surface position x resulting from a unit of slip at ξ on the fault, which is denoted by F. We estimate coseismic slip and the rate of afterslip at the discrete time intervals, 0.0-0.125, 0.125-0.25, 0.5-1.0, 1.0-2.0, 2.0-3.0, 3.0-4.0, and 4.0-5.0 years after the earthquake. Each fault segment is discretized into roughly 4 km by 4 km patches and we estimate a strike-slip and thrust component of slip for each patch. We impose that the direction of slip and slip rate are within 45° of right-lateral. We also add zeroth order Tikhonov regularization so that our solution for s satisfies

$$\min_s \left(\left|\left| \frac{u_{\text{pred}}(s) - u_{\text{post}}}{\sigma_{\text{obs}}} \right|\right|_2^2 + \lambda_s ||s||_2^2 \right). \tag{10}$$

The penalty parameters, λ_s, is chosen with a trade-off curve. We use Pylith **?**,]Aagaard2009 to compute the Green's functions for this inversion and for the remaining inversions in this paper.

Our coseismic slip and afterslip solutions are shown in Figure **??**. As with **?**,]Rollins2015, we find that a large amount of afterslip on the southern fault segment is required to explain the observations. The potency of our inferred coseismic slip is 3.2×10^9 m^3, equivalent to a Mw7.28 earthquake when assuming a shear modulus of

32 GPa. The potency of our inferred cumulative 5 years of afterslip is 6.1×10^9 m^3, equivalent to a Mw7.46 earthquake, which is un-

re- al- is- ti- cally large if we con- sider af- ter- slip to be driven by co- seis- mi- cally in- duced stresses. Our elas- tic slip model ac- cu- rately describes near-field post-seismic de-for-ma-tion, while it sys-tem-at-i-cally un-der-es-ti-mates post-seis-mic de-for-ma-tion for sta-tions further than ~ 150 km from the El Mayor-Cucapah epicentre (Figure **??**). When the fault segments used in the inversion are extended down to 30 km depth, rather than 15 km, the systematic far-field residuals are smaller but remain apparent. Because an elastic model for the lithosphere requires an unrealistic amount of afterslip and is unable to predict far-field deformation, we move on to consider viscoelastic models in the next section.

3.2 constraints on effective viscosity

For any linear viscoelastic rheology of the crust and

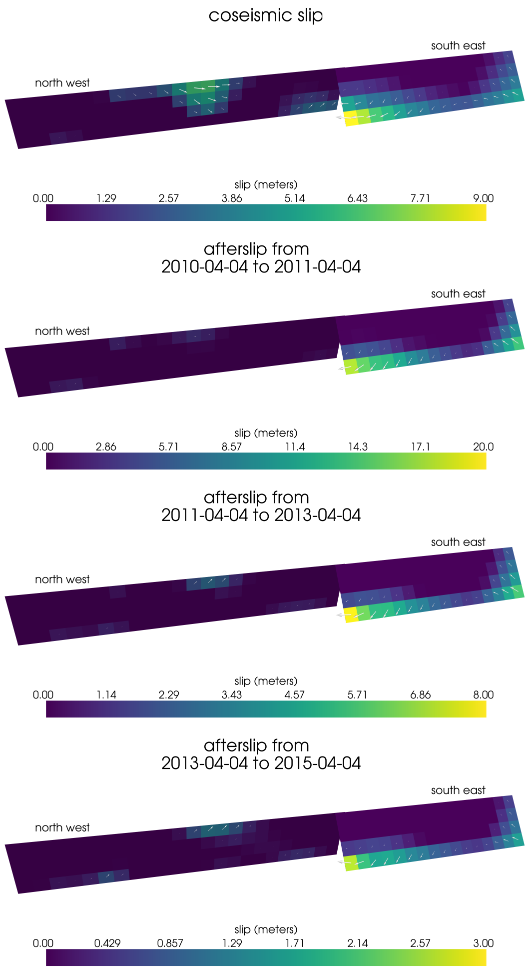

Figure 6. Co-seismic slip and cumulative afterslip over the indicated intervals for the elas-

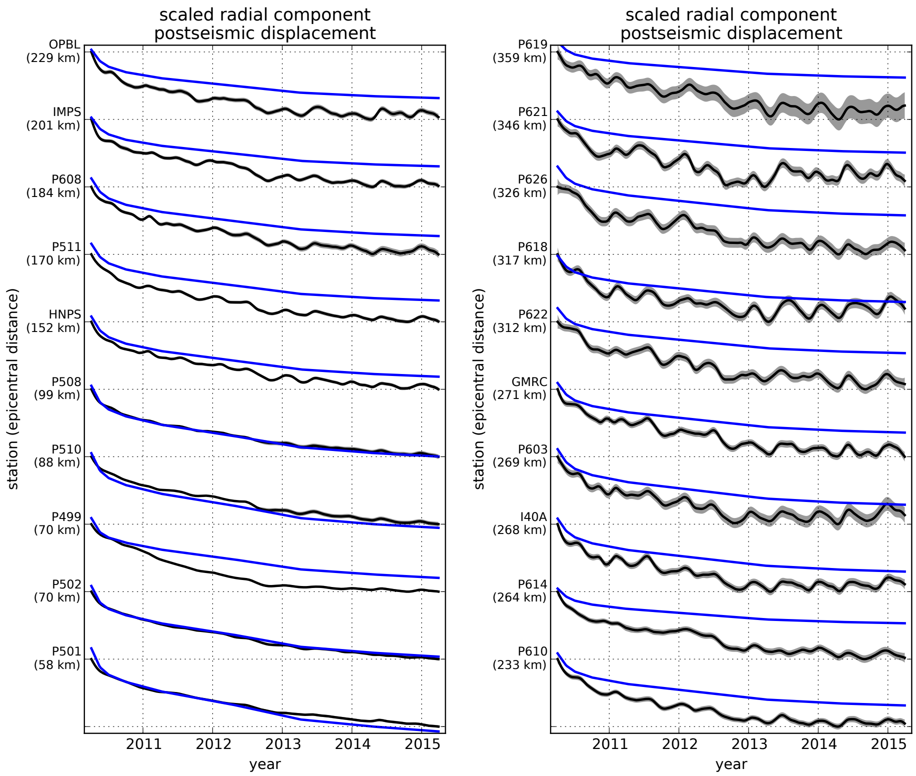

Figure 7. Scaled record section for the radial component of observed postseismic displacements, u_{obs} (black) and displacements pre-

mantle, postseismic displacements resulting from time dependent fault slip can be described as

$$u_{\mathrm{pred}}(x,t) = \int_F s(\xi,t)g(x,\xi)d\xi + \int_0^t \int_F s(\xi,\tau)f(t-\tau,x,\xi)d\xi d\tau \quad (11)$$

where $f(t,x,\xi)$ describes the time-dependent velocity at x resulting from viscoelastic relaxation of stresses induced by slip at ξ. f is a function of λ, μ, and any additional rheologic parameters controlling the viscoelastic response, which are generally not well known. Schematic representations of the vis-coelas-tic rhe-o-logic mod-els con-sid-ered in this study are shown in Fig-ure **??**. We con-sider Maxwell vis-coelas-tic-ity, where the steady-state viscosity, η_M, is unknown, Zener viscoelasticty, where the transient viscosity, η_K, and transient shear modulus, μ_K, are unknown, and Burgers viscoelasticity, where η_M, η_K, and μ_K, are all unknown. We further discuss these rheologic models and their use in geophysical studies in Section **??**.

In order to greatly simplify the inverse problem, we use the method described in **?**,]Hines2016 to constrain an initial ef-

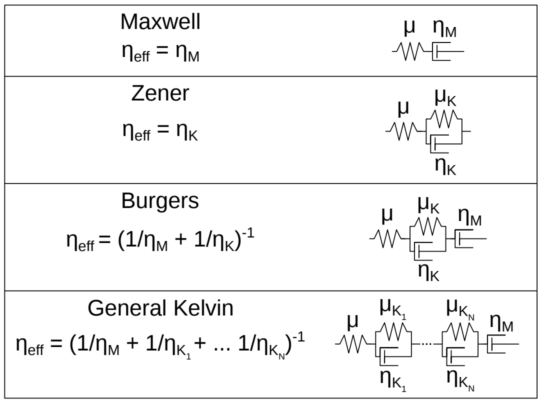

Figure 8. Schematic illustration of rheologic models considered in this paper as well as their initial effection viscosities, $\eta_{\text{eff}} = \frac{\sigma}{\dot{\epsilon}}\big|_{t=0}$.

fec- tive litho- spheric vis- cos- ity struc- ture from the early post- seis- mic de- for- ma- tion. The method re- lies upon the fact that im- me- di- ately af- ter an earth- quake, stresses through- out the crust and man- tle are only con- trolled by the rel- a- tively well known in- stan- ta- neous elas- tic prop- er- ties and each parcel will have a strain rate, $\dot{\epsilon}$, that is proportional to stress, σ, and inversely proportional to the parcel's effective viscosity, $\eta_{\text{eff}} =$

$\frac{\sigma}{\dot{\epsilon}}\Big|_{t=0}$. Through linear superposition, we can deduce that the initial rate of surface deformation resulting from viscoelastic relaxation is a summation of the surface deformation resulting from each parcel, scaled by the reciprocal of the parcel's effective viscosity. That is to say

$$f(0, x, \xi) = \int_L \frac{h(x, \xi, \zeta)}{\eta_{\text{eff}}(\zeta)} d\zeta, \quad (12)$$

where $h(x, \xi, \zeta)$ describes the initial rate of deformation resulting from viscoelastic relaxation at ζ induced by slip at ξ and L denotes the crust and mantle. We can combine eq. (**??**) with eq. (**??**) to get a first order approximation for early postseismic deformation,

$$u_{\text{pred}}(x,t) \approx \int_F s(\xi,t) g(x,\xi) d\xi + \int_0^t \int_F \int_L \frac{s(\tau,\xi)}{\eta_{\text{eff}}(\zeta)} h(x,\xi,\zeta) d\zeta d\xi d\tau, \tag{13}$$

which is valid for as long as the rate of deformation resulting from viscoelastic relaxation is approximately constant. Although eq. (**??**) may only be valid for a short portion of the postseismic period, its utility becomes apparent when noting that g and h are only functions of the fault geometry and instantaneous elastic properties, λ and μ, and so g and h can be computed numerically as a preprocessing step and the forward problem in eq. (**??**) can be rapidly eval-u-ated for any re-al-iza-tion of s and η_{eff}. This is in con-trast to eval-u-at-ing the full forward problem, eq. (**??**), numerically for each realization of s and unknown rheologic properties. Figure **??** shows how estimates of η_{eff} can then be used as a constraint on the unknown parameters for various linear viscoelastic rheologies.

We perform an initial inversion of postseismic displacements using the approximation in eq. (**??**). We estimate coseismic slip and after-slip with the same spatial and temporal discretization as in Section **??**. Simultaneously, we estimate η_{eff} within six vertically stratified layers which have depths ranging from 15-30 km, 30-60 km, 60-90 km, 90-120 km, 120-150 km, as well as from

150 km to the bottom of our numerical model domain at 800 km. We again restrict fault slip to occur between 0 and 15 km

depth and we made this choice to help elim- i- nate in- evitable non unique- ness. It has long been rec- og- nized that fault slip at suf- fi- ciently great depths can produce surface deformation that is indistinguishable from viscoelastic relaxation, at least in two-dimensional earthquake models **?**,]Savage1990. Since we are trying to simultaneously model these two processes, it is necessary to put sensible constraints on the depth of fault slip. Additionally, we note that when simultaneously estimating afterslip in the lower crust and a lower crustal viscosity, the in- verse prob- lem be- comes par- tic- u- larly ill- posed. This ill- posedness is il- lus- trated in Fig- ure (**??**), which shows the dis- place- ments re- sult- ing from a meter of slip on a fault extending from 15 to 30 km depth and the initial velocity resulting from viscoelastic relaxation in the lower crust, which is given a viscosity of 10^{18} Pa s. The horizontal displacements from fault slip are in the opposite direction as the displacements resulting from subsequent viscoelastic relaxation. This means that surface displacements resulting from afterslip at lower crustal depths can be cancelled out, at least partially, by a low viscosity lower crust. We eliminate this null space by al- low- ing only one mech- a- nism in the lower crust, which we choose to be vis- coelas- tic re- lax- ation. This is not to say that we do not believe deep afterslip to be a possibility, rather we restrict slip to seismogenic depths as a modelling necessity. Although, it has been noted that the pattern of vertical postseismic deformation following the El Mayor-Cucpah earthquake indicates that a significant-icant amount of afterslip must be shallow **?**,]Rollins2015.

Further details on how s and η_{eff} are estimated from postseismic deformation

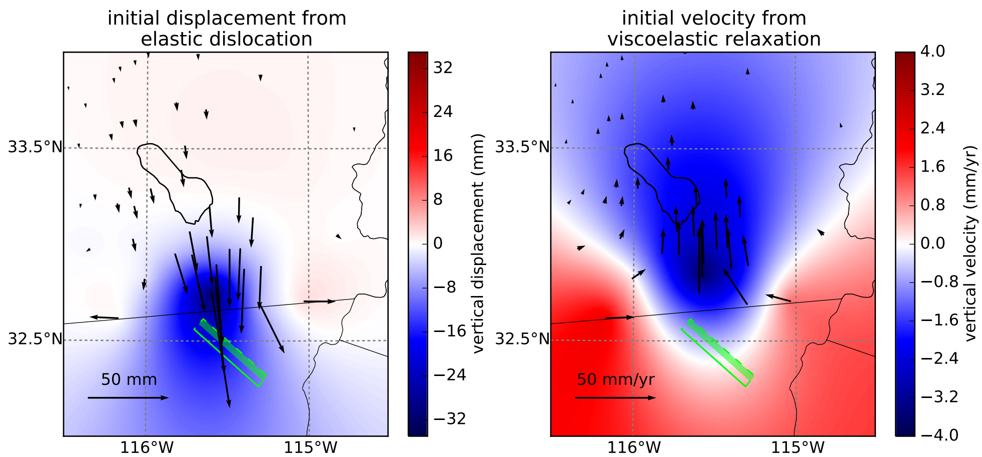

Figure 9. Displacements resulting from fault slip at lower crustal depths (left), and initial velocity resulting from subsequent relaxation of a viscoelastic lower crust

can be found in **?**,]Hines2016. A non-linear Kalman filter based inverse method can also be used to estimate s and η_{eff} in a manner akin to

?,]Segall1997 or **?**,]McGuire2003, in which we would not have to explicitly impose a time dependent parametrization of s. We have thoroughly explored Kalman filter based approaches, but we ultimately prefer the method described in **?**,]Hines2016 because of its relative simplicity. Moreover, we believe the piecewise continuous representation of slip with respect to time to be sufficiently general for the resolving power of these GPS data.

The first step in our inverse method is to determine at which point the early postseismic approximation breaks down, which we will de- note as t_{bd}. As noted, it is valid for ap- prox- i- mately as long as the rate of de- for- ma- tion re- sult- ing from vis- coelas- tic relaxation is approximately constant. We can almost certainly assume that deformation at the most far-field stations, which are $\sim$

400 km away from the El Mayor-Cucapah epicentre, is the result of viscoelastic relaxation. The approximation should then be valid for

as long as a linear trend adequately approximates the far-field deformation. Using this logic, it would appear that $t_{\mathrm{bd}} \approx 1$ year after the El Mayor-Cucapah earthquake. Another way to determine t_{bd} is to find the best fitting prediction of eq. (**??**) to observed deformation using increasing durations of the postseismic time series. t_{bd} should be the point when eq. (**??**) is no longer capable of describing the observed deformation without incurring systematic misfits. This is illustrated in Figure **??**, which show the scaled radial components of displacement for stations along the El Mayor-Cucapah P axis. When using eq. (**??**) to fit the entire 5 years of post-seis-mic dis-place-ment we see that the near-field dis-place-ments, e.g. sta-tion P501, are ac-cu-rately pre-dicted but when look-ing at dis-place-ment in the far-field, e.g. station P621, we see that eq. (**??**) overestimates the rate of deformation in the later post-seismic period and underestimates the rate of deformation in the early period. Due to the low signal-to-noise ratios for far-field stations, it is dif- fi- cult to de- ter- mine at what point eq. (**??**) is no longer able to pre- dict the ob- served dis- place- ments with- out in- cur- ring any sig- nificant systematic misfit; however, we settle on $t_{\mathrm{bd}} = 0.8$ years after the earthquake, while acknowledging that the choice is subjective.

As noted in **?**,]Hines2016, overestimating t_{bd} will result in a bias towards overestimating η_{eff}, while picking a t_{bd} which is too low will not necessarily result in a biased estimate of η_{eff}, although the uncertainties would be larger. We can then consider inferences of η_{eff} to be an upper bound on the viscosity needed to describe the far-field rate of deformation during the first

0.8 years of post-seismic deformation.

We estimate co-seismic slip, afterslip, and effective viscosity by solving

$$\min_{s,\eta_{\text{eff}}} \left(\left\| \frac{u_{\text{pred}}(s,\eta_{\text{eff}}) - u_{\text{obs}}}{\sigma_{\text{obs}}} \right\|_2^2 + \lambda_s ||s||_2^2 + \lambda_\eta ||\nabla \eta_{\text{eff}}^{-1}||_2^2 \right) \tag{14}$$

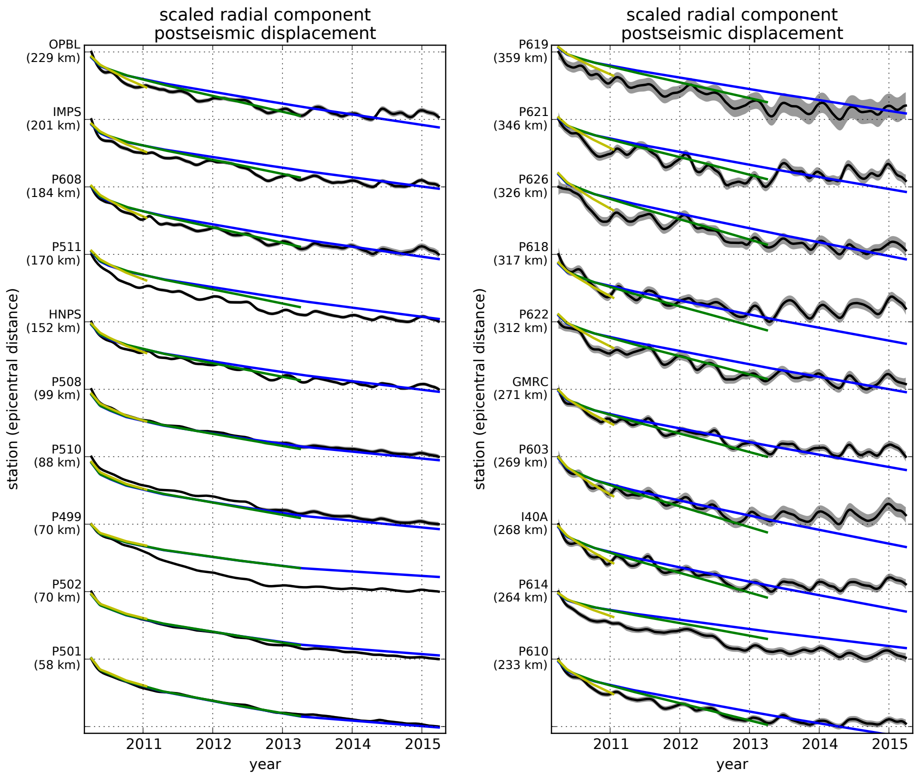

Figure 10. Illustration of how t_{bd} is chosen. Observed postseismic displacements are shown in black. Blue, green and yellow low

where u_{obs} consists of the first 0.8 years of postseismic deformation and u_{pred} are the predicted displacements from eq. (**??**). Due to inherent non uniqueness, we have added zeroth order Tikhonov regularization to estimates of s, and second order Tikhonov regularization to estimates of effective fluidity, η_{eff}^{-1}. The degree to which we impose the regularization on slip and fluidity is controlled by the penalty parameters λ_s and λ_η. The penalty parameters are chosen with two trade-off curves. We first choose λ_s while fixing λ_η at 0 and then we determine λ_η with λ_s fixed at its chosen value. Our goal here is to get a prior constraint on η_{eff} to minimize the amount of searching we have to do when describing the postseismic deformation over the full 5 years, which we do in Section **??**. Estimates of s made here will not be used in Section **??**, and so the motivation behind even adding regularization to s is to ensure that the slip driving viscoelastic relaxation in eq. (**??**) is sensible.

Our inferred estimates of effective viscosities, and corresponding fluidities, are shown in Figure **??** with their 95% confidence intervals indicated, which were estimated through bootstrapping. Although fluidity is rarely used in geophysical literature, eq. (**??**) is linear with respect to fluidity and so the fluidity indicates the amplitude of the viscoelastic signal coming from each layer. We note that the magnitude of the uncertainties on viscosity tend to decrease as we increase λ_η. Our choice of λ_η was based on a standard technique used in geophysical inverse problems which has no statistical backing. It is therefore difficult to interpret the magnitude of uncertainties on viscosities shown in Figure **??**; although, we do believe that the relative uncertainty between layers is accurately depicted. A robust feature that we see is that the largest jump in fluidity is at 60 km depth, which is consistent with the range of lithosphere-asthenosphere boundary depths inferred by **?**,]Lekic2011. This transitional depth is also consistent with the the viscosity structure required to explain far field postseismic deformation following the Hector Mine earthquake **?**,]Freed2007a. We find that the viscosity below low

60 km depth needs to be $\sim 1\times 10^{18}$ Pa s to describe the early rate of postseismic deformation at far-field stations while the lower

crust and uppermost mantle need to be relatively stronger. The viscosity of the lower crust is the least well constrained as there is no evidence of relaxation in that layer, meaning that it is effectively elastic over the first 0.8 years after the earthquake.

Our initial es-

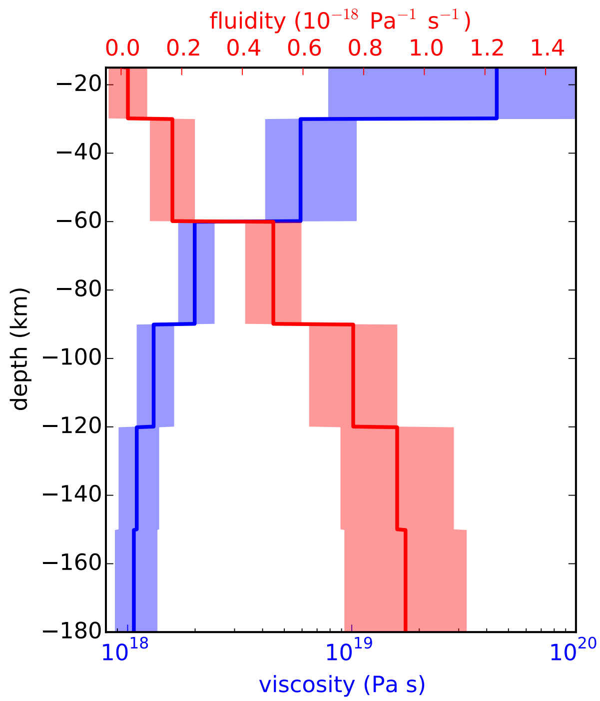

Figure 11. Effective viscosity and associated fluidities inferred by fitting eq. (**??**) to the first 0.8 years of post-

timate for coseismic slip and cumulative afterslip over the first 0.8 years after the El Mayor-Cucapah earthquake are shown in Figure

??. Similar to our elastic slip model from Section **??**, coseismic slip is inferred to be in the Sierra Cucapah and it is right lateral with a significant normal component. This is consistent with field studies **?**,]Fletcher2014, as well as the coseismic slip from

?,]Wei2011. The potency of inferred coseismic slip is 3.3×10^9 m^3, which is also about the same as that inferred from Section **??**. The present inference of afterslip on the Indiviso fault is significantly less than what was found in the Section **??** where we did not account for viscoelasticity. When fault slip is simultaneously estimated with a lithospheric and asthenospheric viscosity, the potency of inferred afterslip over the first 0.8 years after the earthquake is 0.85×10^{9} m^{3}, compared to 3.46×10^{9} m^{3} when we assume the lithosphere and asthenosphere are elastic. The significant amount of afterslip inferred on the Indiviso fault seems to be compensating for unmodelled viscoelastic relaxation at depths greater than 60 km. The fact that there is still an appreciable amount of afterslip inferred on the Indiviso fault even when allowing for viscoelastic relaxation in the lower crust and upper mantle raises the question of whether it is compensating for viscoelastic relaxation that is more localized than what we allow for since we only estimate depth dependent variations in viscosity.

3.3 Full Inversion

In the previous section, we used the inverse method from **?**,]Hines2016 to constrain the effective

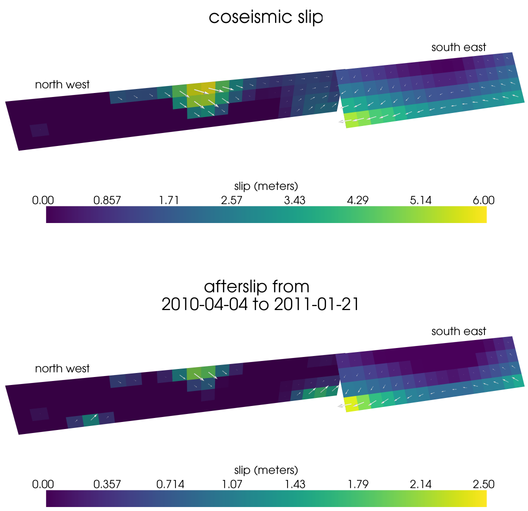

Figure 12. Coseismic slip and afterslip inferred by fitting eq. (**??**) to the first 0.8 years of postseismic displacements.

viscosity structure required to explain the first 0.8 years of postseismic deformation. In this section, we use the effective viscosi- ties in- ferred above as a prior con- straint when search- ing for mod- els which are ca- pa- ble of de- scrib- ing the avail- able 5 years of post- seismic data, where our forward problem is now eq. (**??**) rather than the approximation given by eq. (**??**). We perform a series of coseismic slip and af- ter- slip in- ver- sion as- sum- ing a va- ri- ety of rhe- olo- gies for the lower crust and up- per man- tle which are con- sistent with our findings from Section **??**. We appraise each model using the mean chi squared value,

$$\bar{\chi}^2 = \frac{1}{N} \left|\left| \frac{u_{\mathrm{pred}} - u_{\mathrm{obs}}}{\sigma_{\mathrm{obs}}} \right|\right|_2^2, \tag{15}$$

where N is the number of observations.

We first assume that the crust and mantle can be described with a Maxwell rheology, and we set η_{M} equal to our inference of

η_{eff}. We compute f and g from eq. (**??**) using the finite element software, Pylith **?**,]Aagaard2009, and assume the same spatial and temporal discretization of s as in Sections **??** and **??**. We estimate s using linear least squares and we find $\bar{\chi}^2 = 37.4$. For comparison, $\bar{\chi}^2 = 35.3$ for the elastic model from Section **??**. The Maxwell viscoelastic model has a larger misfit because it tends to overestimate the rate of deformation after about 3 years **??**. Since our initial estimates of η_{eff} may be biased towards overestimating viscosities, we have also performed the slip inversion where we use uniformly lower viscosities in the crust and mantle. However, decreasing the viscosity only increases the misfit. Although, the viscosities used here are consistent with the successful Maxwell viscoelastic models found by **?**,]Rollins2015 and **?**,]Spinler2015, which had mantle viscosities on the order of 10^{18} Pa s, we find that such a model is incapable of describing the entire postseismic time series. **?**,]Pollitz2001 similarly recognized this deficiency in a Maxwell rheology, which then motivated their exploration of a Burgers rheology upper mantle **?**,]Pollitz2003.

Rather than exploring a Burgers rheology mantle, which introduces two new parameters that need to be estimated, η_K and μ_K, we first consider a Zener rheology for the mantle, which only introduces the unknown parameter μ_K. We assume that the lower crust still has a Maxwell rheology. The steady-state viscosity, η_M, in the crust and the transient viscosity, η_{K}, in the mantle are set equal to the inferred effective viscosities. We then estimate the ratio of shear moduli, $\frac{\mu_K}{\mu}$. We compute nine different sets of Green's functions, f and g, using Pylith, where we assume values of $\frac{\mu_K}{\mu}$ ranging from 0 to 1. The former being a degenerate case where the Zener model reduces to the above Maxwell model. We estimate coseismic slip and afterslip for each realization of $\frac{\mu_K}{\mu}$. The shear moduli ratio that yields to best prediction to the observed postseismic displacements is found to be 0.375 with a misfit of $\bar{\chi}^2 = 31.2$ (Figure **??**). The improvement in the Zener model over the Maxwell model can be clearly seen in the fit to the far-field data (Figure **??**). The Zener model does a significantly better job at explain-ing the transient rate of far-field deformation throughout the 5 years.

Because we are able to adequately describe the available 5 years of

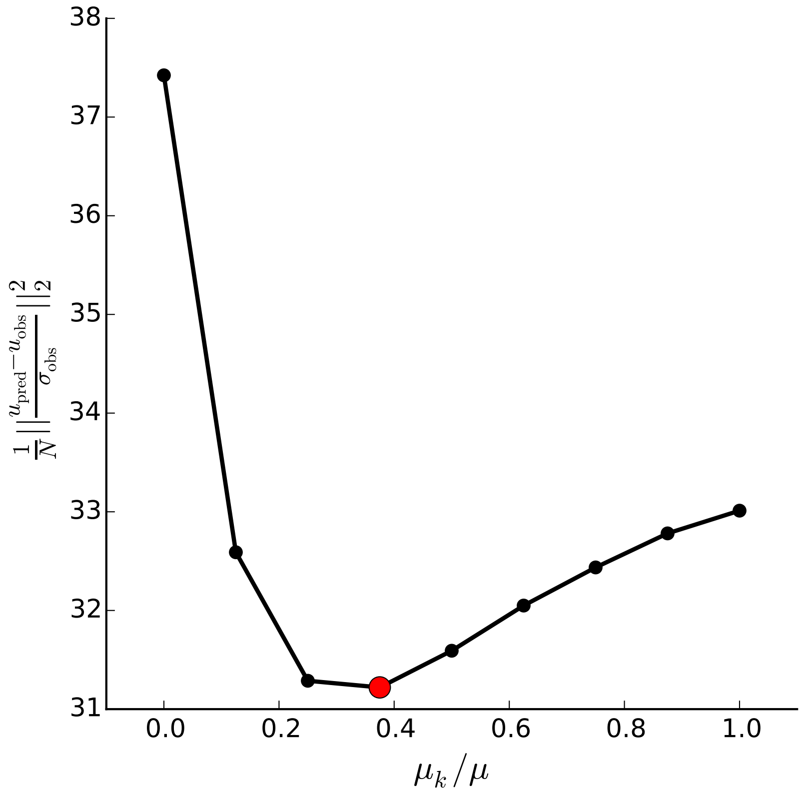

Figure 13. Misfit as a function of the transient shear modulus in a Zener rheology upper mantle.

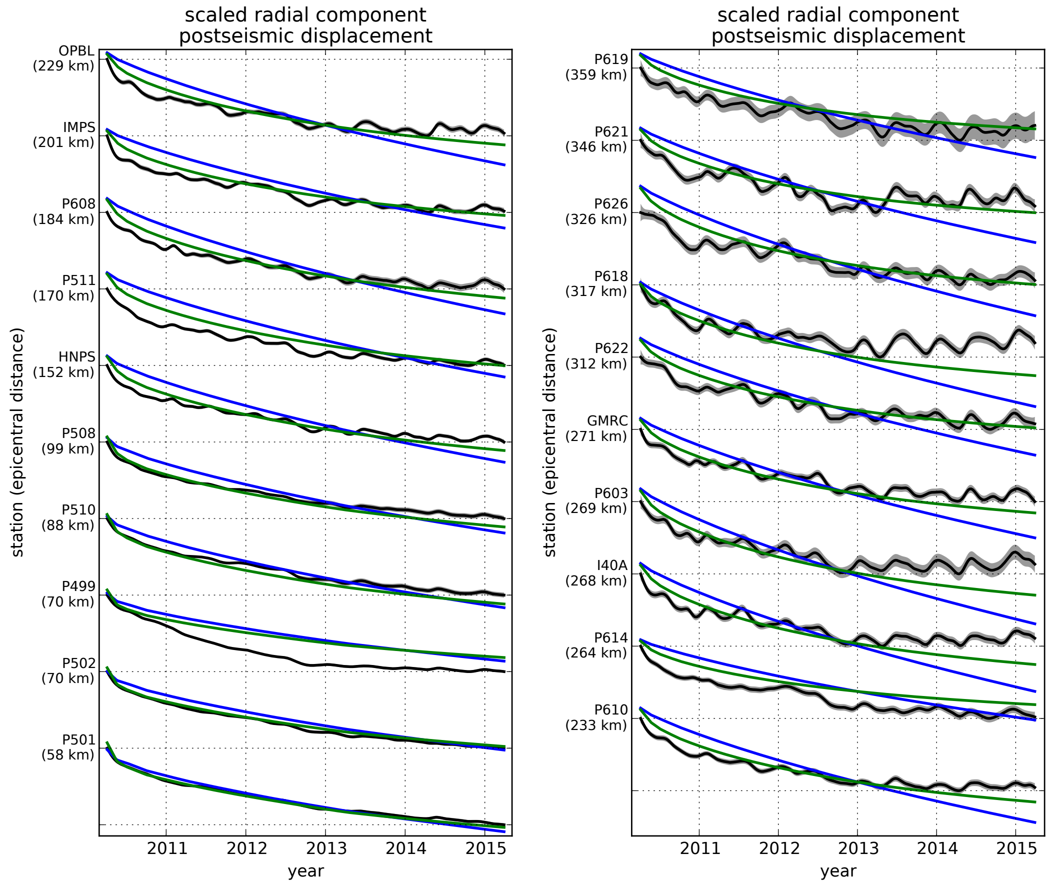

Figure 14. Observed postseismic displacements (black) and predicted postseismic displacements for the best fitting slip

postseismic deformation with a Zener model, we do not find it necessary to explore the parameter space for a more complicated Burgers rheology. However, since the Zener model is a Burgers model with an infinite steady-state viscosity, we can conclude that any

Burgers rheology that has a transient viscosity consistent with that found in Section **??** and a steady-0state viscosity of $\gtrsim$ 10^{20}

Pa s, which is effectively infinite on the time scale of 5 years, would also be able to satisfactorily describe the observable postseismic deformation.

The regularized inference of coseismic slip and afterslip for our preferred Zener model is shown in

Figure **??** and the predicted postseismic displacements are shown Figures **??**, **??** and **??**. Overall, the trends in the near-field and far-field transient deformation are accurately described by our preferred model. In particular, the trends in far-field deformation are much better described by our preferred Zener model than either an elastic model or a model with a Maxwell viscoelastic mantle (Figure **??**). There are a few areas where we have notable misfit. Most of our misfit is for the near-field stations in the Imperial Valley, and we attribute this misfit to our relatively simple fault geometry, which does not account for potential fault slip in the Imperial Valley triggered by the El Mayor-Cucapah earthquake **?**,]Wei2011a,Wei2015. In particular, we are unable to model the sustained rapid rate of deformation at station P496, which suggests that this station could be influenced by a more localized deformation mechanism than is considered in this study. Additionally, we see systematic misfit in the later postseismic period west of the location of the Landers and

Hector Mine earthquakes, which may be the result of unmodelled postseismic deformation resulting from those earthquakes. Lastly, there are clear discrepancies between the observed and predicted vertical deformation following the first year after the El Mayor Cucapah earthquake. We observe a broad uplift throughout Southern California, which is inconsistent with any postseismic model.

The inferred co-

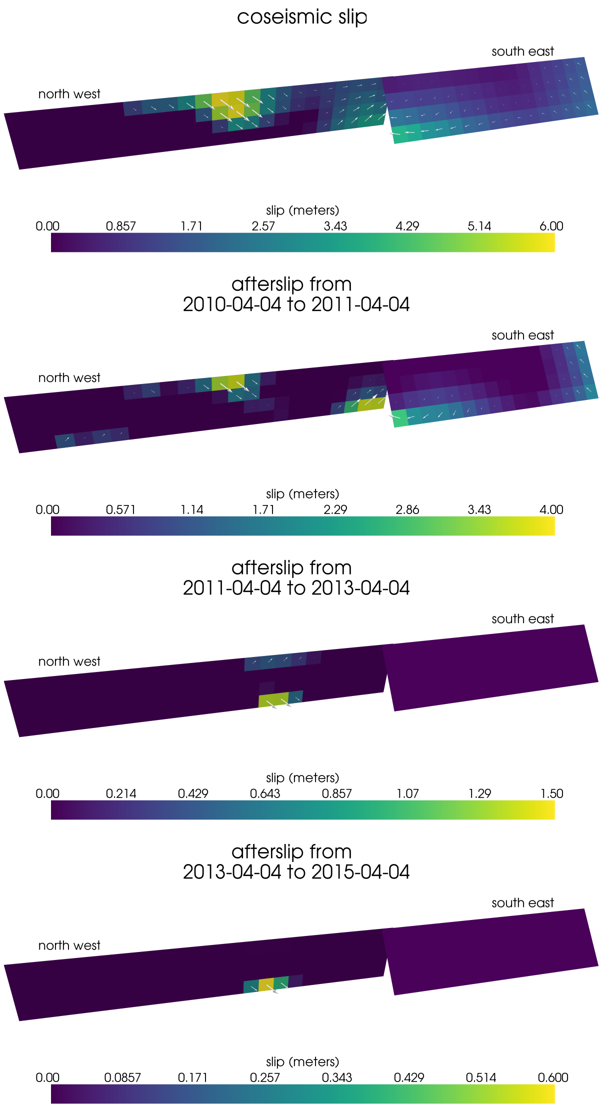

Figure 15. Inferred coseismic slip and afterslip when assuming a Maxwell rheology

seismic potency is 3.0×10^9 m^3, equivalent to a Mw7.26 earthquake, and the potency of 5 years of afterslip is 1.1×10^9 m^3. Most of the afterslip in our preferred model occurs within the first year after the earthquake with a significant amount inferred to be shallow and in the Sierra Cucapah. The afterslip within the first year is accounting for the most rapid near-field transient deformation. After 1 year, afterslip is inferred to be deeper and under the Sierra Cucapah, which is describing much of the sustained near-field postseismic deformation. We emphasize, that the GPS station closest to our inferred afterslip, P496, is still about 30 km away, which is too far away for us to conclusively argue for sustained brittle deformation rather shallow ductile deformation. The deep afterslip inferred after 1 year could potentially be describing deformation resulting from lower crustal flow. To test this, we have modified our preferred model by decreasing the lower crustal viscosity from 5.91×10^{19} Pa s to 1×10^{19} Pa s, which is still consistent with our viscosity inference from Section **??**. After performing another slip inversion, we find that a model with a weaker lower crust adequately describes the post-seismic displacements without any afterslip after 1 year, while still requiring about the same amount of afterslip over the first year. We do believe that the early shallow afterslip is a robust feature in our preferred model, while we are not confident in our inference of later deep afterslip.

4 Discussion

It has long been recognized that deep afterslip and viscoelastic relaxation following-ing an upper crustal earthquake can result in similar horizontal ground deformation at the surface **?**, e.g.]Savage1990, Pollitz2001,Hearn2003,Feigl2006. The similarity of the horizontal postseismic deformation results in a non-uniqueness in inferences of afterslip or viscoelastic relaxation. In contrast, the spatial pattern of vertical postseismic deformation has been proposed to be a discriminant between deep afterslip and viscoelastic relaxation **?**, e.g.]Pollitz2001, Hearn2003. It is, however, important to note that patterns of vertical cal deformation are very sensitive to the depth-dependence of viscosity below the upper crust **?**,]Yang1981, Hetland2014. The similarity between deformation resulting from deep afterslip and viscoelastic relaxation of coseismic stresses is different from the ill-posedness described in Section **??**. In our method, any inferred afterslip will also mechanically drive additional viscoelastic relaxation. The horizontal deformation resulting from deep afterslip will generally be in the opposite direction as horizontal deformation resulting from viscoelastic relaxation of subsequent stresses in the lower crust (Figure **??**). As a result, there is a trade-off between inferences of deep afterslip and lower crustal viscosity. In our synthetic tests in **?**,]Hines2016, we have found that inverting surface deformation for afterslip and viscosity within the same depth interval tends to result in overestimated afterslip and an underestimated viscosity at that depth.

Most postseismic studies assume Maxwell viscoelasticity in the lower crust and upper mantle **?**, e.g.]Nur1974,Pollitz2000,Hetland2003,Freed2006a,Johnson2009,Hearn2009, which is the simplest viscoelastic rheologic model. In Southern California, postseismic studies following the Landers **?**,]Pollitz2000, Hector Mine **?**,]Pollitz2001, and El Mayor-Cucapah earthquake **?**,]Spinler2015,Rollins2015, have assumed Maxwell viscoelasticity in the lithosphere and asthenosphere and have inferred upper mantle viscosities on the order of 10^{17} to 10^{18} Pa s and lower crust viscosities of $\gtrsim 10^{19}$ Pa

s. These postseismic studies are corroborated by **?**,]Kaufmann2000 who found that a lower crust and upper mantle with viscosities on the order of 10^{20} and 10^{18} Pa s, respectively, are necessary to describe subsidence resulting from Lake Mead, which is a process with similar spatial and temporal scales as postseismic deformation. While these studies found viscosities that are consistent with our effective viscosities from Section **??**, they are inconsistent with viscosity estimates made from geophysical processes that occur over longer time scales. For example, **?**,]Lundgren2009 found that lower crust and upper mantle viscosities on the order of 10^{21} and 10^{19} Pa s, respectively, are needed to describe interseismic deformation along the Southern San Andreas and San Jacinto fault. An even higher mantle viscosity on the order of 10^{20} Pa s is required to describe deflection resulting from Lake Bonneville, which occurs on the time scales of 10^4 years **?**,]Crittenden1967,Bills1987.

An additional deficiency with the Maxwell rheology is that it predicts a steady decay over time in the rate of post-seismic deformation, which fails to describe the commonly observed rapid early transience followed by a relatively steady rate of post-seismic deformation. One could explain the early transient post-seismic deformation with fault creep and the later phase with relaxation in a Maxwell viscoelastic lower crust and upper mantle **?**, e.g]Hearn2009,Johnson2009. However, postseismic deformation at distances greater than $\sim$ 200 km from the El Mayor-Cucapah epicentre can only be attributed to viscoelastic relaxation **?**,]Freed2007a and we have demonstrated that the far-field deformation cannot be explained with a Maxwell rheology (Figure **??**).

We found that a Zener rheology in the upper mantle with a transient viscosity of $\sim 10^{18}$ Pa s does a noticeably better job at predicting far-field postseismic deformation. A generalization of the Zener viscoelastic model, schematically represented as several Kelvin elements connected in series, is commonly used to describe seismic attenuation **?**,]Liu1976. The highest viscosity needed to describe seismic attenuation is on the order of 10^{16} Pa s **?**,]Yuen1982 which has a characteristic relaxation time on the order of days. Even though our inferred transient viscosity is orders of magnitude larger than that required for seismic attenuation models, the two models are not incompatible. Rather, the delayed elasticity in seismic attenuation models occurs on such short time scales that it can be considered part of the instantaneous elastic phase of deformation associated with the preferred Zener model in this study.

Of course, it has long

been recognized that a Zener rheology provides an incomplete descriptions of the asthenosphere, as it does not have the fluid-like behaviour required to explain isostatic rebound or convection in the mantle **?**,]OConnell1971. **?**,]Yuen1982 proposed a Burgers rheology with a low transient viscosity ($\eta_K \approx 10^{16}$ Pa s) and high steady-state viscosity ($\eta_M \approx 10^{21}$ Pa s) to describe both seismic attenuation and long term geologic processes. The justification of a Burger's rheology mantle is further supported by laboratory experiments on olivine **?**,]Chopra1997. **?**,]Pollitz2003 sought to describe postseismic deformation following Hector Mine with a Burgers rheology mantle and they found a best fitting transient viscosity of 1.6×10^{17} Pa s and steady-state viscosity of 4.6×10^{18} Pa s. While the Burgers rheology was introduced as a means of bridging the gap between relaxation observed in long and short term geophysical processes, the inferred steady state viscosity from **?**,]Pollitz2003 is still inconsistent with the Maxwell viscosities inferred from earthquake cycle and lake load- ing stud- ies. The tran- sient vis- cos- ity in- ferred by **?**,]Pol- litz2003 is con- strained by the ear- li- est phase of post- seis- mic de- for- mation following the Hector Mine earthquake. While **?**,]Pollitz2003 ruled out deep afterslip as an alternative mechanism based on inconsistent vertical deformation, it is still possible to successfully describe all components of early postseismic formation fol- low- ing the Hec- tor Mine earth- quake with af- ter- slip at seis- mo- genic depths **?**,]Ja- cobs2002. It is then pos- si- ble that the pre- ferred rheologic model from **?**,]Pollitz2003 was biased towards inferring a particularly low transient viscosity by neglecting to account for afterslip. This is in contrast to the present study, where we have inferred a lithospheric viscosity structure simultaneously with afterslip. We also argue that a transient rheology is necessary to explain postseismic deformation; however, our preferred transient viscosity of $\sim 10^{18}$ Pa s in the mantle is an order of magnitude larger than the transient viscosity found by **?**,]Pollitz2003. Since a Zener model is able to describe the available post-seismic deformation following the El Mayor-Cucapah earthquake, any Burgers rheology with a steady-state viscosity that is $\gtrsim 10^{20}$ Pa s, effectively infinite over 5 years, would also be able to describe the postseismic deformation. Such a Burgers model might then be consistent with the steady state viscosities necessary for lake loading, interseismic deformation, and mantle dynamics.

5 Conclusion

We have extracted a filtered and smoothed estimate of postseismic deformation following the El Mayor-Cucapah earthquake from GPS displacements time series. We have treated postseismic deformation as a stochastic process where we did not presume any characteristic shape of the post-seismic time series. We can observe transient post-seismic deformation at distances of $\sim$ 400 km from the El Mayor-Cucapah epicenter which is largely undetectable after about 3 years. Near-field deformation exhibits transience that decays to a sustained, elevated rate after about 1 to 2 year. We found that the near-field transient deformation can be explained with shallow afterslip and the sustained rate of near field deformation can either be explained with continued afterslip or relaxation in a lower crustal with a viscosity of $\sim 10^{19}$ Pa s. Far-field transient deformation can be more definitively ascribed to viscoelastic relaxation at depths greater than $\sim$ 60 km. Beneath that depth, a transient viscosity of $\sim$ 10^{18} Pa s is required to describe the rate of far-field deformation throughout the 5 years considered in this study. By describing the available post-seismic deformation with a transient rheology in the mantle, our preferred model does not conflict with the generally higher steady-state viscosities inferred from geophysical processes occurring over longer time scales.

Acknowledgements

We are grateful to Andy Freed for an

illuminating discussion on the material in this manuscript.

This material is based on EarthScope Plate Boundary Observatory data

services provided by UNAVCO through the GAGE Facility with support from the National Science Foundation (NSF) and National Aeronautics and

Space Administration (NASA) under NSF Cooperative Agreement No. EAR-1261833.

This material is based upon work supported by the National Science Foundation under Grant Numbers EAR 1045372 and EAR 1245263.